Tubular parametric volume objects: Thickening a piecewise smooth 3D stick figure

Samuel Peltier, Géraldine Morin, Damien Aholou

Version of Record: https://www.sciencedirect.com/science/article/pii/S0167839621000261
Manuscript_60c0fd5abe4b49bf07622003ca24c76e

Tubular Parametric Volume Objects: Thickening a Piecewise Smooth 3D Stick Figure

Samuel Peltier[a], Géraldine Morin[b], Damien Aholou[a]

[a] *Université de Poitiers, Laboratoire XLIM, Axe ASALI, CNRS 7252, France*
[b] *Université de Toulouse, Laboratoire IRIT, France*

Abstract

In this paper, a volume parametric model is computed from a piecewise smooth skeleton. Generating a volume model from a stick figure S defined in 3D is an intuitive process: given S whose topology is a pseudo-graph and whose edges are embedded as Bézier curves in $\mathbb{R}^3$, we propose a method for creating a thick volume parametric model "around" S. The volume model we generate is based on semi-simploidal sets, which guarantees a proper topology and provides a 3D parametric domain for Bézier spaces. This volume is a continuous piecewise Bézier representation which boundary corresponds to a B-Rep made of tensor product Bézier patches.

Keywords: Tubular objects, Topological based geometric modeling, Bézier volumes, Semi-simploidal sets

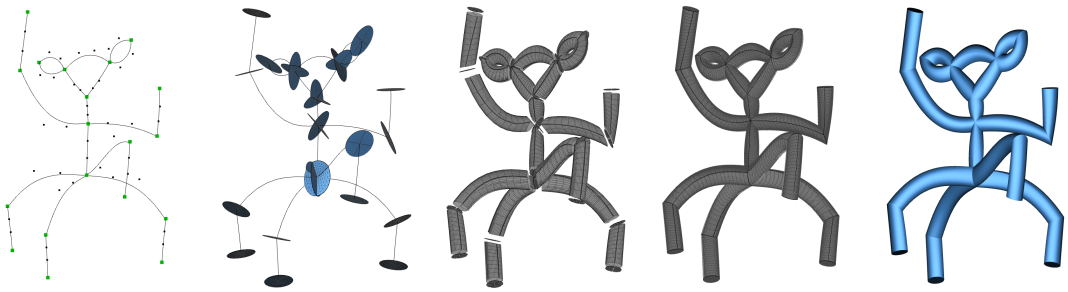

Figure 1: **A parametric volume model from a stick figure.** (*a*) input: a stick figure, a connected set of Bézier curves; (b) Volume junctions computed at each skeleton vertex; (*c*) volume branches; (*d*) a embedded semi-simploidal set defines a topologically coherent parametric domain for volume Bézier patches. (*e*) output: a piecewise smooth parametric volume model.

1. Introduction

Different geometric models are used to represent 3D objects. In particular, Boundary-representations (B-rep) consists in representing a volume object by its outer surface. The parametric surface models based on Bézier, B-splines or NURBS are the standard models used in the kernel of CAD systems (e.g. Farin (2014)). They offer the possibility of studying and ensuring the required smoothness of the 3D geometric surfaces while providing an intuitive control and easy sampling when needed. Their piecewise linear version,

Email addresses: samuel.peltier@univ-poitiers.fr (Samuel Peltier), geraldine.morin@irit.fr (Géraldine Morin), damien.aholou.pro@gmail.com (Damien Aholou)

meshes, have been the most classical representation since they are the natural input of rendering pipelines and the support of texture mapping. They are used in applications where smoothness is not required (e.g. games, e-commerce). More recently, IGA (isogeometric analysis) (see Cottrell et al. (2009) and Hughes et al. (2005)) have proposed to use the geometric model directly for CAM (Computer Aided Manufacturing) based on finite elements computations. With the development of additive manufacturing (3D printing) volume models are needed for representing the geometry of the printed object. When physical properties of a volume object have to be controlled and analyzed (e.g. in the context of additive manufacturing, or 3D printing), a complete volume subdivision has to be handled (i.e. with volume cells) (see Livesu et al. (2017)). Thus, methods for representing the entire volume of an object are in active demand and research. Discrete methods generating volume meshes have been proposed (e.g. Lyon et al. (2016) extract a volume mesh given its surface). Massarwi and Elber (2016) propose a continuous and smooth parametric volume representation based on B-splines; they consider tensor product volume and rely on trimming. These differentiable volume models may be used as support for mechanical computations (see Massarwi et al. (2019)).

A skeleton offers an intuitive, simplified and low-dimensional representation of a 3D object structure. It is thus of interest for shape retrieval (see e.g. Sundar et al. (2003)), shape design in sketching and for animation (see e.g. Raptis et al. (2011)). Bridging the gap between skeletons and corresponding surface models has been targeted by different work Bærentzen et al. (2012) and more recently Usai et al. (2016); Panotopoulou et al. (2018); Fuentes Suárez and Hubert (2018). Livesu et al. (2016) generalize these approaches for computing a volume hexahera mesh from a skeleton.

The goal of this work is to tackle the limitations of the previous methods, by providing a complete framework for generating automatically a piecewise polynomial parametric tubular volume object from an arbitrary skeleton. Compared to Livesu et al. (2017) that generates a piecewise linear model (3D mesh) for a skeleton, we generate a smooth model based on polynomial elements. Moreover, whereas Massarwi et al. (2019) use volume trimming to propose a smooth volume model, we ensure a consistent topology of the domain so that our model is an assembly of well connected complete volume Bézier patches. More precisely, we associate each edge of the skeleton with a volume *branch*, and each vertex of the skeleton with a *branch junction*. The generated tubular volume object is then defined as an assembly of branches that are glued together continuously at branch junctions. Our work generalizes and extends to **smooth parametric volumes** the results presented in Panotopoulou et al. (2018) that creates a surface quad mesh. In their work, all branches of the surface have the same regular structure: a branch surface is only made of four quads. A similar regularity is provided by the proposed volume model: each volume branch has a regular structure. More precisely, each branch is an assembly of four prisms which boundary is also made of four quads (the four prisms are arranged symmetrically around the branch axis). Note that our method offers the possibility to handle branches made of four hexahera, preserving regularity but generating twice as many quads on the surface.

In order to create a parametric model, we use semi-simploidal sets (see Peltier et al. (2009)): a combinatorial structure in which cells (simploids) are products of simplices; in particular, prisms and hexahera are 3D simploids. Adjacency relations are encoded by face operators, and their structure is designed for embedding semi-simploidal sets into simploidal Bézier spaces (i.e. products of simplicial Bézier spaces).

In this paper, we tackle both topological and geometric issues regarding branches, and branch junctions. The main contributions in this paper are the following:

- Regarding the topology:
  - We provide definitions of branches and kites (branch extremities) based on semi-simploidal sets. Our branch definition uses prisms and preserves the minimal number of quad boundary patches (i.e. four). Moreover, we extend this property for Bézier volumes model: all branches have a same volume structure and are bounded by only four quads.
  - The topology of a junction defines how branches are glued together "around" a corresponding vertex of the skeleton. The problem of handling junction configurations is equivalent to the problem of partitioning a unit sphere into quads. We provide a proof showing that any quadrangulation of a sphere can be generated iteratively by inserting quads.

- Regarding the geometry:
  - During the construction of a quadrangulation on a sphere defining the topology of a junction, we propose an incremental algorithm for positioning automatically the quads vertices. Subsequently, all Bézier volume control points at the junctions are placed.
  - We describe how to control the geometry of branches in order to both minimize twisting and preserve a consistent volume along the branch axis. This step places the intermediate Bézier volume control points.

The two following sections of the paper construct the building blocks of the model: the volume branches, and the junctions. Section 2 presents stick figures, the notions and underlying topological structures related to tubular volume branches are detailed. Then Section 3 is dedicated to the topology of junctions. A general iterative process enables the construction of arbitrary junctions. Section 4 describes the complete 3D model construction and focuses on geometric issues regarding junctions and branches. Finally, we show some volume models generated from stick figures with our automatic process.

2. From a Stick Figure to a Volume Tubular Object

In this section, we first introduce the building blocks of the tubular object and discuss how they are intuitively built from a stick figure. The topological nature of tubular volume model is the combinatorial structure of semi-simploidal sets. We recall the basics on this combinatorial structure, and show its benefits for handling both topology and geometry of stick figures and tubular volume objects.

2.1. Building blocks of the tubular object: Stick Figure, Branches and Kites

In this paper, a *stick figure* denotes a skeleton embedded into 3D. More precisely, the structure of a stick figure is a *pseudograph*, i.e. it may contain multi-edges or loops. The embedding of a stick figure is an assembly of Bézier curves: each vertex of the pseudo graph is associated with a $3D$ point, and each edge is associated with a Bézier curve of arbitrary degree.

The idea behind creating the tubular volume object around the stick figure is to thickening the 1D structure into a volume model. Regarding the structure, an edge of the stick figure corresponds to a elementary volume object, denoted as a *branch*. Regarding the embedding, each Bézier curve C of the stick figure is associated with a smooth (volume) branch whose central curve corresponds to C, and each vertex of the stick figure corresponds to a *junction* of branches. Otherwise said, our tubular objects are assemblies of smooth branches that are glued along their extremities.

Each branch is an assembly of 4 prisms sharing a common edge (Figure 2(a)). Each branch is thus bounded by 4 smooth square surface faces and has two extremities made of an assembly of 4 triangles, denoted as a *kite*. Branches are then assembled along kites according to the algorithm presented in Section 4. In our setting, at a kite a branch is incident to up to 4 other branches.

So, the topological structure of a branch consists in an assembly of 4 prisms, 8 square faces (4 are inside, 4 are on the boundary), 8 triangle face, 21 edges, and 10 vertices. All these cells correspond to a same kind of regular cells: simploids Dahmen and Micchelli (1982). Intuitively, a simploid can be seen as the product of (any) simplices. Assemblies of simploids can be handled using semi-simploidal sets: a combinatorial structure for handling simploidal Bézier spaces. More precisely, simploids are a natural domain for Bézier volumes, and so, represent non linear, polynomial models.

Note that, a volume branch could also be defined by a set of four hexahedra and benefit from a semi-simploidal set representation, leading to a coherent topology and a (tensor-product) Bézier embedding, as shown in Figure 2(b). In order to keep the property of having a minimal number of surface patches shown in Panotopoulou et al. (2018), we thus chose to define branches as assemblies of prisms. However, despite having twice as many surface patches (i.e. eight), all our work and proposal does directly carry through with 4-hexahedra branches.

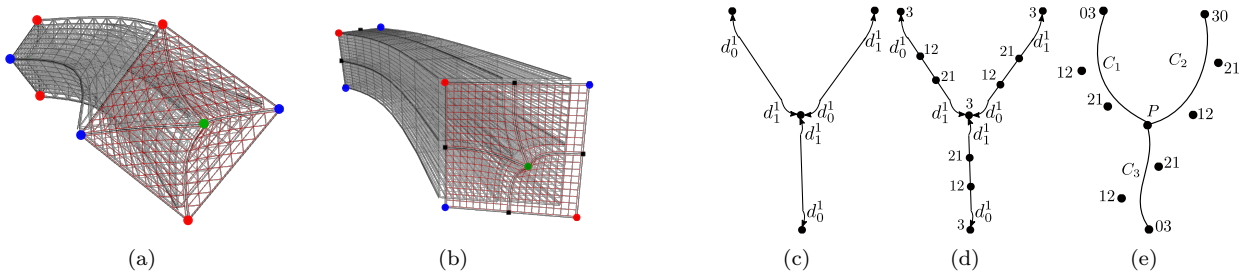

Figure 2: (a) A volume branch which domains are prisms has 4 quad patches on its outer boundary. (b) A volume branch which domains are hexahedra has 8 quad patches on its outer boundary. $(c)-(e)$ an example of a stick figure represented as an assembly of 3 Bézier curves sharing a common vertex. (c) its topology is encoded by a semi-simploidal set of dimension 1. (d) numbering of control points induced by face operators. (e) embedding of the stick figure. Note that the control point P is common to the three curves, and its numbering on each curve depends on the face operators: P is numbered 30 for C_1 and C_3 as it corresponds to the face d_1^1 of C_1 and C_3, whereas P is numbered 03 for C_2 as it corresponds to the face d_0^1 of C_2. Note that Bézier curves have the same degree in this example, but different degrees can be handled.

2.2. Semi-simploidal Sets

The topological structure of our proposed volume model is based on semi-simploidal sets. This combinatorial structure is designed to define assemblies of Bézier volume patches and is the building block of the proposed volume model. In this section, we recall their definition (Section 2.2.1) and their Bézier embedding (Section 2.2.2).

Abstract simplicial complexes Munkres (1984) are the most well-known structure for representing simplicial objects. Within this structure, simplices are defined as sets of vertices. Semi-simplicial sets or $\Delta-$complexes Eilenberg and Zilber (1950); Hatcher (2002) also describe simplicial objects, but in these structures, simplices are defined as sequences of vertices; such structures allow in particular to handle simplicial objects with multi-incidence (for example, an edge loop or two triangles sharing their 3 edges). Semi-simplicial sets are defined as a set of abstract cells (simplices) together with face operators satisfying some properties that ensure a consistent topology. Structural relations have been established between face operators and control points of triangular Bézier spaces Lang and Lienhardt (1996), leading to the definition of data structures allowing to handle the topology of free-form objects, while benefiting from a built-in parametric domain.

In a similar way, semi-cubical sets Brown and Higgins (1981) have been defined for handling assemblies of cubes (i.e. products of edges). More recently, semi-simploidal sets Peltier et al. (2009) have been defined in a similar way for handling assemblies of Bézier simploids DeRose et al. (1993). Intuitively, a simploid Dahmen and Micchelli (1982) corresponds to a product of any simplices, so simplices and cubes are particular simploids.

In the following, we recall the definition of semi-simploidal sets, and their relations to corresponding Bézier spaces (see Peltier and Lienhardt (2018) for theory and implementation details). We then define stick figures, branches and kites using semi-simploidal sets.

2.2.1. Combinatorial structure

A semi-simploidal set is a combinatorial structure, defined as a set of simploids equipped with face operators. A simploid σ is characterized by its type $(a_1, \ldots, a_n)$, where a_i corresponds to the dimension of its i^{th} generating simplex, and $a_i > 0$ for any $1 \leq i \leq n$ (intuitively, the cartesian product of a simplex σ by a vertex, i.e. a simplex of dimension 0, is σ). The dimension k of σ is $\sum_{i=1}^{n} a_i$, i.e., the sum of the dimensions of its generating simplices, and the face operators associates σ with its faces (i.e. simploids of dimension $k-1$). For example, a square is a simploid of type $(1,1)$, thus dimension 2, as it corresponds to the product of two edges, its faces are simploids of type (1) i.e. edges. A prism is a simploid of type $(2,1)$, thus dimension 3, as it corresponds to the product of a triangle by an edge. The faces of a prism are simploids type (2) (i.e. triangles) and $(1,1)$ (i.e. squares), both have dimension 2. Note that a simplex and a cube of dimension k are particular simploid of type (k) and $(1, \cdots, 1)$ with length k respectively.

Definition 1. *A semi-simploidal set $S = (K, (d^i_j))$ is a set of simploids K equipped with a type operator $\mathcal{T} : K \to \bigcup_{i=0}^{\infty} \mathbb{N}^{*i}$ and face operators d^i_j. Let $\sigma \in K$; $\sigma\mathcal{T}$ is the type of σ. Let $\sigma\mathcal{T} = (a_1, \cdots, a_n)$: σd^i_j is defined if $1 \leq i \leq n, 0 \leq j \leq a_i$. Operators satisfy:*

(I) **Action on the type**

$$\sigma d^i_j \mathcal{T} = \begin{cases} (a_1, ..., a_i - 1, ..., a_n) \text{ if } a_i > 1 \\ (a_1, ..., a_{i-1}, a_{i+1}, ..., a_n) \text{ otherwise} \end{cases}$$

(II) **Commutation of face operators**

$$d^i_j d^i_l = d^i_l d^i_{j-1} \quad l < j, a_i > 1$$
$$d^i_j d^k_l = \begin{cases} d^k_l d^i_j & \text{if } a_k > 1 \\ d^k_l d^{i-1}_j & \text{otherwise} \end{cases} \qquad k < i$$

The face operator d^i_j associates with σ the same product of simplices, except that the i^{th} generating simplex is replaced by its j^{th} face. So, the type of σd^i_j is $(a_1, \cdots, a_i - 1, \cdots, a_n)$ if this j^{th} face is not a vertex, $(a_1, \cdots, a_{i-1}, a_{i+1}, \cdots, a_n)$ otherwise. Note that σd^i_j denotes $d^i_j(\sigma)$.

In this work, stick figures (i.e. graphs), are handled by semi-simploidal sets of dimension 1 (cf. Figure 2$(c) - (e)$). For the volume model, only one type of simploid of dimension 3 is used: prisms. Let σ be a prism, then σ is equipped with 5 boundary operators: d^1_0, d^1_1, d^1_2 which point to its three faces of type $(1, 1)$ (i.e. square faces) and d^2_0, d^2_1 which points to its two faces of type (2) (i.e. triangles). Commutation properties guarantee a consistent topology. For example, the square face σd^1_1 and the triangle face σd^2_0 share the common edge $\sigma d^1_1 d^2_0 = \sigma d^2_0 d^1_1$ (cf. Figure 3(b)).

2.2.2. Bézier Embedding

In addition to a consistent topological structure, semi-simploidal sets also offer a domain for Bézier volume shape. This section briefly recalls the general setting, and highlights the specific Bézier elements the branches are made of.

A simploidal Bézier space is a set S of Bézier simploids such that the intersection of any two simploids σ and τ of S is either empty or a simploid of S, corresponding to a common face of σ and τ.

The set Γ^i_d of *i-dimensional multi-indices of degree d* is defined by $\Gamma^i_d = \{\alpha = (\alpha_0, \cdots, \alpha_i) \in \mathbb{N}^{i+1} \mid |\alpha| = \alpha_0 + \cdots + \alpha_i = d\}$. *Multivariate Bernstein polynomials of degree d* are defined at v by $B^d_\alpha(v) = \binom{d}{\alpha} v_0^{\alpha_0} \cdots v_i^{\alpha_i}$, with $\alpha \in \Gamma^i_d$, and $\binom{d}{\alpha} = \frac{d}{\alpha_0! \cdots \alpha_i!}$ are *multinomial coefficients*, and $\{v_j\}$ are the barycentric coordinates of v, a point of the standard i-simplex, i.e. $\{v_j\}$ satisfies: $\forall j, 0 \leq j \leq i, 0 \leq v_j \leq 1$ and $\sum_{j=0}^{i} v_j = 1$. A Bézier simploid of type $(a_1, \ldots, a_n)$ and degree $(d_1, \ldots, d_n)$ is defined by:

$$P(u^1, \ldots, u^n) = \sum_{\alpha^1 \in \Gamma^{a_1}_{d_1}} \cdots \sum_{\alpha^n \in \Gamma^{a_n}_{d_n}} P_{(\alpha^1, \ldots, \alpha^n)} B^{d_1}_{\alpha^1}(u^1) \times \ldots \times B^{d_n}_{\alpha^n}(u^n)$$

where any u^i is a point of the standard a_i-simplex and $\{P_{(\alpha^1, \cdots, \alpha^n)}\}$ is its set of control points.

A semi-simploidal set structure can be associated with a simploidal Bézier space, as a direct correspondence exists between a semi-simploidal set and the structure of its control points. This correspondence is based on the fact that for any control points of a Bézier simploid σ having a zero on a given multi-index position, means that it also corresponds to a control point of a Bézier simploid of the boundary of σ. Moreover, the position of the zero corresponds to the index of the face operator.

In our setting (see Figure 3 $(c) - (d)$), we consider prism μ of type $(2, 1)$ and degree $(3, 3)$. The only control points that are inside μ are $P_{(111,12)}$ and $P_{(111,21)}$; the sets of control points $\{P_{(\alpha^1,03)}\}$ and $\{P_{(\alpha^1,30)}\}$ correspond to their triangular face μd^2_0 and μd^2_1 respectively.

2.3. Semi-simploidal Branches and Kites

As mentioned before, branches are built by "gluing" four prisms together as illustrated in Figure 2(a). Gluing corresponds more formally to an identification operation (see Peltier et al. (2009) Section 3.2.2. for details). Identifying two simploids and their boundary consists in merging them into a single simploid, according to their orientation (induced by face operators). Regarding branches, each prism shares a common quad face with each of its two neighbors. The identification operation will be also used when branches

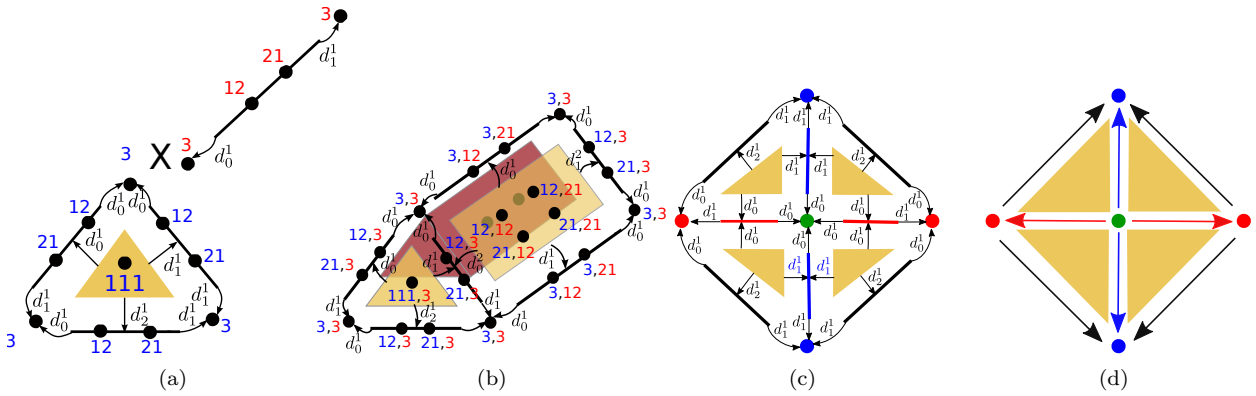

Figure 3: $(a) - (b)$: Correspondences between control points of a Bézier prism and its face operators represented by arrows. The prism μ on (b) (and its faces) is the product of the triangle σ_1 (and its faces) and the edge σ_2 (and its faces) on (a). The square face represented on (b) is $\mu d_1^1 = \sigma_1 d_1^1 \times \sigma_2$; the bottom square face of μ is $\mu d_2^1 = \sigma_1 d_2^1 \times \sigma_2$; the square face on the back side is $\mu d_0^1 = \sigma_1 d_0^1 \times \sigma_2$; the front triangle face is $\mu d_0^2 = \sigma_1 \times \sigma_2 d_0^1$; the back triangle face is $\mu d_1^2 = \sigma_1 \times \sigma_2 d_1^1$. The prism contains only two proper control points of the volume $P_{111,12}$ and $P_{111,21}$; all other control points are also control points of a Bézier simploid of dimension 2, 1 or 0. (c) a kite, the extremity of a branch, is a semi-simploidal set of dimension 2. This specific assembly of 4 prisms leads to symmetries on the kite. (d) simploid coloration is sufficient to recover the face operators of a kite.

are glued along part of their kites. Topological correctness of each branch ensures the correctness of the corresponding Bézier structures. As a consequence, two incident Bézier prisms share a common Bézier quad surface, and the central Bézier curve is a single curve object shared by the four Bézier prisms and the four inside Bézier quad surfaces. Note that Bézier prisms are defined by volume control points.

On top of the four outer surface boundary quad, a branch now has two extremities, called *kites*. Figure 3(c) illustrates the simploidal structure of these kites. Our specific assembly of 4 prisms ensures that kites have an interesting property of axial symmetry regarding simploid orientations (see. Figure 3(d)). Thus, to each vertex of the stick figure corresponds a set of kites in the volume object, assembled into a so called *kite folio*.

3. Handling Topology of Junctions

In this part, we provide all the material for generating *any* branch junction corresponding to a vertex of a stick figure, through an iterative process. Whereas this section concentrates on the arrangement of branches, filling in the corresponding volume is addressed in Section 4.

We consider a unit sphere around each vertex v of degree $n \geq 2$ of the stick figure: each edge incident to v is embedded as a Bézier curve, and its tangent at the vertex defines an exit ray which meets the sphere in one point; we denote these points *green points*. A quad tessellation (or quadrangulation) of this sphere is built incrementally while considering branches at this junction. Then each branch extremity is plugged onto its corresponding quad in the quadrangulation.

3.1. Simple Quadrangulations on a Sphere: Properties and Orientation

In this paper, we consider *simple quadrangulations* on a sphere (or SQS for short): a class of simple planar graphs (i.e. with no self loop nor double edges) such that each face is bounded by four vertices. Simple quadrangulations on surfaces have been studied in Nakamoto (1996). Batagelj (1989) studies classes of quadrangulations generated by inductive definitions, i.e. starting from an initial configuration and generating rules (adding quads). Following this approach, Brinkmann et al. (2005) defines *expansions* operations and their inverse, *face reductions* involving only vertices of minimal degree 2 or 3. In fact he defines special case of the general *face contraction* operation defined in Nakamoto (1996). Roughly speaking, these operations consist in adding or removing a quad while preserving a quadrangulation. He shows that any SQS can

be reduced to the minimal one, made of only two faces, by a sequence of face reductions applied to faces incident to a vertex of minimal degree.

Panotopoulou et al. (2018) also investigate the problem of generating SQS. Their approach is based on splitting quads, which corresponds one expansion operation of Brinkmann et al. (2005). Indeed, in the resulting quadrangulation, at least 2 quads share 2 adjacent edges, so at least two branches are twice incident to each other. As a consequence, configurations where each branch has four different neighbors can not be obtained, e.g. the surface of a dice involving six branches (see Figure 5 $(d) - (f)$). Such configurations are important, in particular, when the six branches join in the six canonical, orthogonal directions.

In our context, where expanding and reducing a quad corresponds to adding or removing a branch of the volume object, it is essential to be able to chose the location of the quad. In the following, we provide all the necessary properties to prove Theorem 1. In terms of graph generation our result is similar to the one of Brinkmann et al. (2005), but the proof we provide is more relevant for geometric consideration since it is based on the fact that in an SQS with $n > 2$ quads, any chosen quad can be reduced (Proposition 6).

Properties of SQS

Note that a *SQS* is bipartite, and the length of any cycle in a *SQS* is even, and is greater or equal to 4.

Property 1. *Let Q be a SQS having $n \geq 2$ quads. If $n = 2$, then the two quads share their 4 edges, else two quads of Q do not share opposite edges.*

Proof. Let us consider a SQS having $n > 2$ faces, and F_1, F_2 be two of its faces. Let us assume that F_1 and F_2 share 2 opposite edges. Thus F_1 and F_2 share the same 4 vertices. As F_1 and F_2 do not share their 4 edges, there is at least one double edge, which is a contradiction with the definition of a SQS (which contains no multi-edge). □

As a direct consequence, the following properties hold:

Property 2. *In a SQS having $n > 2$ quads, any two quads share at most 2 (adjacent) edges.*

Property 3. *Let (a, b, c, d) be a quad of a SQS such that b and d have a neighbor vertex in common (different from a and c). Then, a and c do not have any neighbor vertex in common (different from b and d).*

Proof. Let us assume that both a and c have a common neighbor vertex v, and b and d have a common neighbor vertex w.

- Let us assume that $v = w$. A *SQS* is bipartite, so a, c and w have the same color and b, d and v the other color. So v and w have different colors, so v can not be equal to w, which leads to a contradiction.
- Let us assume $v \neq w$. The boundary of the quad (a,b,c,d) is by definition also the boundary of the rest of the SQS. Any two paths linking a to c in one hand, and b and d on another hand must intersect as they are opposite vertices of a quad, but the only vertex in these two paths are v and w, and $v \neq w$ which leads to a contradiction.

□

Property 4. *Let Q be a SQS with $n > 2$ quads, and let (a, b, c, d) be a quad of Q such that b and d do not have a neighbor vertex in common (different from a and c). Then, a and c have at least degree 3.*

Proof. If b or d has degree 2, then property 2 ensures that a and c have at least degree 3. If b and d have at least degree 3, then let us assume that a has degree 2, then the second face containing a also contains b and d, thus b and d must have a common vertex. Which leads to a contradiction. The same result holds for d. □

In practice, SQS vertices, edges and faces (here *quads*) are handled through the combinatorial structure of oriented maps which provides orientation of cells of the subdivision (also used in Section 4). In the following, we define expansion and reduction of quads for oriented maps, namely *opening* and *closing*.

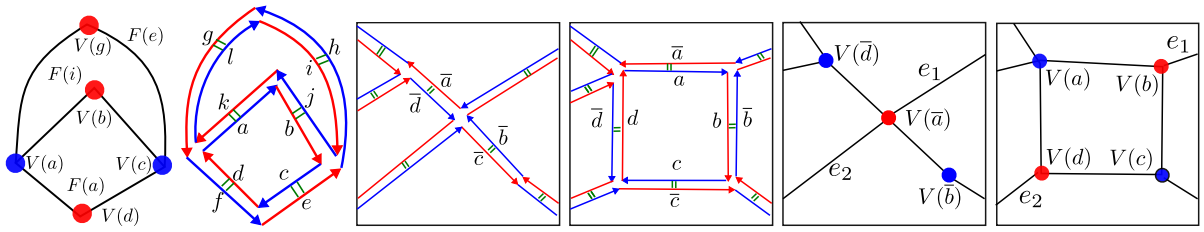

(a) (b) (c) (d) (e) (f)

Figure 4: (a) : a SQS with 3 faces, 6 edges, and 5 vertices. (b) : its corresponding oriented map with 12 darts labelled from a to l. Each dart is represented by an arrow, which direction encodes permutation β_1; involutions β_2 are represented in green between two opposite darts. $(c) - (d)$: Focus on a quad. From (c) to (d): opening operation relatively to darts $\overline{a}$ and $\overline{c}$. From (d) to (c): closing operation relatively to dart a (or c).SP(e), (f): the SQS corresponding to (c) and (d) respectively. Note that after opening: $V(\overline{d}) = V(a)$ and $V(\overline{b}) = V(c)$.

Oriented Maps

Oriented maps are designed to represent any subdivision (not necessarily quad faces) of orientable surfaces without boundaries. The concept was first introduced by Edmonds (1960), and is also known as *half-edge* (see. Weiler (1985); Mäntylä (1988)) ; it has been extended for orientable or not orientable surfaces by Guibas and Stolfi (1985), to dimension 3 by Dobkin and Laszlo (1987), to any dimension by Vince (1983); Lienhardt (1989). Equivalence between these structures has been shown in Lienhardt (1991). Interested readers can find more details about such structures in Damiand and Lienhardt (2014).

Definition 2. *An oriented map is a triplet (H, β_1, β_2) where H is a finite set of elements called darts, β_1 is a permutation on H, and β_2 is an involution on H.*

Intuitively, within this structure, each edge is decomposed into two opposite darts (also called half-edges). Each dart h is associated with a unique vertex, edge, and face denoted $V(h)$, $E(h)$ and $F(h)$ respectively. All vertices, edges and faces correspond to cycles $\beta_2\beta_1$, β_2 and β_1, respectively. In other words, 2 opposite darts corresponding to the same edge are linked by involution β_2, while the permutation β_1 allows to traverse the boundary of a face, and permutation $\beta_2\beta_1$ allows to turn around each vertex. For example, on Figure 4(b), face $F(a) = F(b) = F(c) = F(d)$ is defined by the permutation (a, b, c, d); edge $E(a) = E(k)$ by the permutation (a, k); vertex $V(c) = V(h) = V(j)$ by the permutation (c, h, j). By definition, each face of the map corresponds to an elementary cycle in the corresponding SQS Q.

Since Q is bipartite, we can color its vertices blue and red. Note that each dart is associated to a unique vertex, hence a red or blue color can be associated to each dart, according to its corresponding vertex as shown in Figures 4(a) and 4(b).

3.2. Opening and Closing operations

In the following, *SQS oriented map* denotes an oriented map corresponding to a SQS. Figure 4 illustrates an opening (Definition 3, from c to d) and a closing (Definition 4 from d to c).

Definition 3. *Let $Q' = (H', \beta'_1, \beta'_2)$ a SQS oriented map, and $\overline{a}, \overline{c} \in H'$ s.t. $V(\overline{a}) = V(\overline{c})$. Let $\overline{d} = \overline{a}\beta_2$ and $\overline{b} = \overline{c}\beta_2$, the* ***opening*** *$(Q', \overline{a}, \overline{c})$ is the SQS oriented map $Q = (H, \beta_1, \beta_2)$ defined by :*

- $H = H' \cup \{a, b, c, d\}$
- $\forall h \in H', h\beta_1 = h\beta'_1$;
- $a\beta_1 = b; b\beta_1 = c; c\beta_1 = d; d\beta_1 = a$, *that is, (a, b, c, d) is the new quad;*
- $\forall h \in H' - \{\overline{a}, \overline{b}, \overline{c}, \overline{d}\}, h\beta_2 = h\beta'_2$;
- $\overline{a}\beta_2 = a$; $a\beta_2 = \overline{a}$; $\overline{b}\beta_2 = b$; $b\beta_2 = \overline{b}$; $\overline{c}\beta_2 = c$; $c\beta_2 = \overline{c}$; $\overline{d}\beta_2 = d$; $d\beta_2 = \overline{d}$.

Definition 4. *Let $Q = (H, \beta_1, \beta_2)$ a SQS oriented map with $n > 2$ quads, and (a, b, c, d) a quad of Q such that $V(b)$ and $V(d)$ do not have a common neighbor vertex other than $V(a)$ and $V(c)$. We denote $\overline{a} = a\beta_2$, $\overline{b} = b\beta_2$, $\overline{c} = c\beta_2$ and $\overline{d} = d\beta_2$. The **closing** (Q, a) is the SQS oriented map $Q' = (H', \beta'_1, \beta'_2)$ defined by:*

- $H' = H - \{a, b, c, d\}$
- $\forall h \in H', h\beta'_1 = h\beta_1$;
- $\forall h \in H' - \{\overline{a}, \overline{b}, \overline{c}, \overline{d}\}, h\beta'_2 = h\beta_2$;
- $\overline{a}\beta'_2 = \overline{d}$; $\overline{d}\beta'_2 = \overline{a}$; $\overline{b}\beta'_2 = \overline{c}$; $\overline{c}\beta'_2 = \overline{b}$.

Note that the *opening* operation is the inverse of the *closing* operation. This can easily be checked by applying directly the definitions. Note also that *closing(Q,a)* is equivalent to *closing(Q,c)*. An important result (Property 6) is that any quad (a, b, c, d) can be closed along at least one of its two diagonals (a, c) or (b, d).

Property 5. *Let $Q = (H, \beta_1, \beta_2)$ be a SQS oriented map, $a, c \in H$ and $Q' = closing(Q, a)$. Then Q' is a SQS oriented map.*

Proof.
1. In Definition 4, the precondition ensures that $V(b)$ and $V(d)$ do not have any neighbor vertex in common. So, Property 4 ensures that $V(a)$ and $V(c)$ have both degree at least 3. So the corresponding vertices in Q' have same degree minus one, which remains ≥ 2. Moreover, $V(b)$ and $V(d)$ are merged in Q' into a single one having degree $deg(V(b)) + deg(V(d)) - 2$, which is by definition also ≥ 2. So **all vertices of Q' have degrees greater or equal to** 2.
2. All the faces of an oriented map are cycles β_1. According to Definition 4, no β_1 is modified, so all faces keep the same number of edges in their boundary after the operation. As Q' is obtained from a SQS Q, **all the faces of Q' remain quads**.
3. By construction, the two vertices that are merged are opposite points (same color) of a quad, so **no loop can appear after a closing**.
4. The only multi-edge that could be created are the one incident to $V(b)$ and $V(d)$ before the operation. This would be the case if these two vertices share a common neighbor vertex, but the precondition states that they do not share a common neighbor vertex. So Q' **contains no multi edge**.

□

3.3. Generating any SQS with a sequence of openings

The closing operation has been defined in order to prove Theorem 1.

Property 6. *In a SQS having $n > 2$ quads, any quad can be closed.*

Proof. The proof is a direct consequence of Property 3 and Property 4. □

Property 7. *The SQS having $n = 2$ quads can be obtained from any SQS by any sequence of closing operations.*

Proof. Property 6 ensures that for any SQS with $n > 2$ quads, any quad can be closed. As a direct consequence, given an arbitrary SQS with $n > 2$ quads, $n - 2$ quads can be iteratively chosen and closed to obtain a SQS with $n = 2$ quads. □

We can now establish the following theorem, which ensures that any SQS can be obtained with a sequence of openings:

Theorem 1. *Any SQS having $n \geq 2$ quads can be obtained from the canonical SQS having 2 quads, by performing a sequence of $n - 2$ openings.*

Proof. The proof is straightforward using Property 7 and the fact that opening is the inverse of closing. □

From a SQS, a surface tubular object can be created by matching each branch boundary to its corresponding quad. In the process of creating a complete volume object, the next section goes one step further by connecting the volume branches inside the junction spheres, leading to a continuous volume object.

4. Creating a Complete Tubular Volume Model and Defining its Geometry

In the two previous sections, we have shown how to define the topology of the 3D model from the stick figure. Namely, Section 2 defines the 3D branches, and Section 3 shows how to generate an SQS for handling junctions of arbitrary topology: the SQS is built incrementally at each junction, by a sequence of openings. This sequence corresponds to an ordering on the green points inherited from an incremental construction of stick figure.

In this section, we create the topology of the complete volume model and automatically define its geometry by positioning of its control points. Section 4.1 describes how the topology of the volume object is defined: first a kite folio is generated from the SQS, then all branches are plugged into corresponding kites according to a chosen red and blue coloring. Section 4.2 focuses on the geometry: the first part addresses junctions and the second one branches.

4.1. Topology of the 3D Model

As mentioned before, to each vertex of the stick figure corresponds a junction of volume branches. We denote these volume junctions *kite folio* (cf. Figure 1 (b)). We establish the following process for building the topology of a tubular object from a stick figure:

- When adding a curve to the stick figure, each extremity of the corresponding branch is inserted into SQS, giving the opening support. Once all curves have been processed, an SQS is built around each vertex (Section 3);
- Then, from an SQS, a kite folio is computed. This kite folio ensures a continuous junction of the volume branches, connecting their extremities (kites) within the sphere;
- Now, each branch needs to be connected to its corresponding kite. Before linking the kite folios by plugging branches, a traversal of the stick figure propagates a red/blue coloration of junction SQSs.

Below, we detail the last two points.

From an SQS to a kite folio

At the end of the construction of an SQS Q (with a green point hosted in each quad), Q can directly be converted into a semi-simploidal set S of dimension 1 such that each edge $e = (v_{red}, v_{blue})$ in Q is mapped to an edge σ of S, such that $\sigma d_0^1 = \mu$ and $\sigma d_1^1 = \mu'$ where μ and μ' corresponds to v_{red} and v_{blue} respectively.

Then, a kite folio can directly be obtained by applying a *cone* operation[1] on S with a new vertex v, which we choose to be the sphere center. More precisely, the kite folio is defined as follows: for each edge σ (resp. vertex μ) of S, a new triangle $\overline{\sigma}$ (resp. edge $\overline{\mu}$) is added, such that: $\overline{\mu} d_0^1 = v$, $\overline{\mu} d_1^1 = \mu$, $\overline{\sigma} d_2^1 = \overline{\sigma}$, $\overline{\sigma} d_0^1 = \overline{\sigma d_0^1}$, and $\overline{\sigma} d_1^1 = \overline{\sigma d_1^1}$. Note that this operation creates a semi-simploidal set of dimension 2 such that all triangles are incident to v. Figure 3(c) illustrates the cone operation on a single quad boundary of Q with the green central vertex: each internal edge $\overline{\mu}$ comes from a red or blue vertex μ; its face d_0^1 is the green vertex, and its face d_1^1 is μ. Similarly, each triangle $\overline{\sigma}$ comes from an edge σ of the boundary quad, which is its face d_2^1; its faces d_0^1 and d_1^1 are the internal edges $\overline{\mu}$ which comes from σd_0^1 and σd_1^1 respectively. The cone on S with v, the sphere center, results in a kite folio (see Figure 5 (e)): as any edge is shared by exactly two quads in Q, any triangle of the kite folio is shared by exactly two kites. Otherwise said, each triangle is the support for a "quarter of" two branches (one on each side).

Applying this process to an entire stick figure generates a set of kite folios intuitively connected by the stick figure curves (see Figure 1 (b)).

[1] The general cone operation is not recalled here, (see Peltier et al. (2009), Section 2.2.1. for details.)

Plugging branches into the set of kite folios

As a branch is plugged into its kite through an identification, the vertex colors have to be matched (as explained in Figure 3(c)). So, a red (resp. blue) vertex of the branch kite is matched with one of the two red (resp. blue) vertices of its corresponding kite in the kite folio. It is sufficient to select only one (red or blue) point, identification of the two kites follows directly; thus, this offers two possible kite identifications.

Moreover, we have an extra degree of freedom per junction: on a kite folio, red and blue vertex colors can be swapped. Swapping the colors on a kite folio changes the orientation of the four triangles of all kites (as illustrated on a single kite on Figure 3(d)). To determine sequentially the choice of color at each junction, we traverse the stick figure by a BFS (breadth first search) starting at the node of maximum depth (degree one stick graph vertices and loops are considered depth zero) and maximal degree. The color of this first kite folio is arbitrary, but then, a coloring is chosen for each traversed kite folio, according to geometric criteria based on branch orientation detailed in section 4.2.2.

4.2. Geometry of the 3D Model

Now that we have addressed all topological considerations for creating a complete model, this section addresses geometric considerations for embedding the complete model in 3D.

A direct user based option for positioning the branches at junctions could directly be implemented: while building a stick figure, the user chooses a sequence of openings for each junction, and sets the position of each red and blue vertex in the corresponding junction. Then, the internal control points of the branch can be also positioned. Such a solution provides entire control of the structure and geometry of each branching, but it may take a lot of interactions to build a volume object corresponding to a stick figure.

4.2.1. Geometry of junctions

Given the sequence of openings that generates an SQS Q and then a kite folio, we now explain the heuristic we propose for positioning red and blue vertices of Q at each step. To achieve this goal, we rely on Q^* the dual of Q, whose vertices are the green points, and faces correspond to red and blue points.

Dual of an SQS

Let Q be an SQS, we define the *pinching* operation in Q^*, corresponding to an *opening* in Q (see Figure 5). The motivation for considering Q^*, the dual of Q, comes from the fact that the positions of the (green) vertices are determined by the stick graph. In Section 4.2.1, given those green points, we determine where to place the red and blue vertices of Q.

Note that Q^* is a planar graph, like Q, but is not an SQS. In practice, Q^* is also represented by an oriented map. Q^* has the following properties:

- The faces of Q^* inherit an orientation from Q;
- Q^* is not simple: when two quads of Q share two incident edges, Q^* has a double edge, thus a $2-$sided face. Note that Q^* can not have any loop since Q has no degree 1 vertex;
- Q^* is 4-regular: the faces of Q are quads, so each green vertex of Q^* is incident to exactly four edges.

Junctions are built using a sequence of openings: in practice, the corresponding dual pinching operations are processed in the dual oriented map representing Q^*.

Choice of pinching

At each step of an SQS construction, a new edge from the stick figure is considered, thus a new green vertex g is added on the sphere. This new vertex g belongs to exactly one face f of Q^*. Considering the position of g (which is fixed by the stick figure) in f, a pinching operation is determined by the choice of two edges of f. Intuitively, these chosen edges are each split into two edges adjacent to g, splitting the face f into two faces (Figure 5 $(a)-(c)$). The choice of the two edges to pinch is based on two criteria:

- a connectivity criterion: in order to balance the number of edges in the resulting faces, we select the edges to pinch on opposite sides of the face. Note that choosing two adjacent edges would create a new double edge in Q^*.

- a geometry criterion: in an attempt to create faces with comparable surface areas, we select edges that update faces so that their change in surface area after pinching is the most comparable.

In practice, it is unlikely to select a face f bounded by a double edge unless the new vertex g lies exactly on the geodesic line between its 2 vertices. However, the heuristic we propose tackles this issue: once f (with 3 or more vertices) is determined, we check if any edge e of f is a double edge. Then, if it is the case, and if e is closer to g than the center of f, the 2-sided face bordered by e is selected for the pinching instead of f.

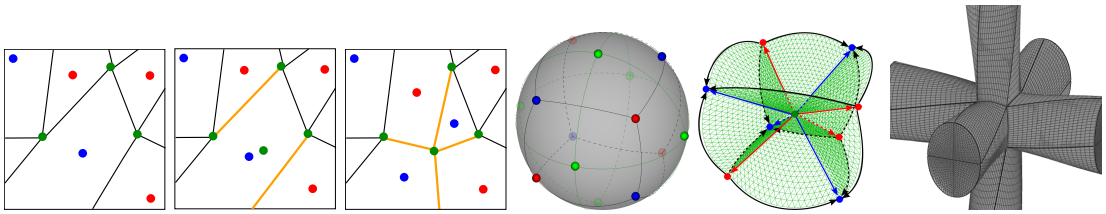

(a) (b) (c) (d) (e) (f)

Figure 5: $(a)-(c)$: **pinching on** Q^* of two edges of a face corresponds to an opening on Q. (a): Q^* with n green points. (b) adding a new green vertex on the face of a blue point and choosing the two edges in Q^* to be pinched (in orange). (c) result of the pinching creates a new face in Q^*. $(d)-(e)$: **The dice configuration**. (d): an SQS (red and blue points) Q in "dice" configuration together with its dual (green points). (e) applying a cone operation on the 1D semi-simploidal set S obtained from Q with the sphere center generate a kite folio. (f): the same dice configuration with volume branches.

Placing the red and blue vertices

Now that Q^* is entirely defined, we describe how red and blue vertices of Q are placed on the sphere during the sequence of pinchings. Remember that red and blue vertices of Q corresponds to faces in Q^*, and faces in Q^* are bounded by 2, 3 or more green vertices. At the beginning of the process, we consider first two green points, thus the corresponding SQS corresponds to the base case of two branches, where the 4 points (2 blue, 2 red) are distributed on the plane bisector of the two green points (such junction with two branches appears on Figure 1 (b)). Then, for junctions with more than 2 branches, for each new green vertex that is added, we place the red and blue vertices on the sphere, at a so-called *center* of a face of Q^* depending on its number of vertices:

- For faces bounded by two green vertices (those are bounded by a double edge of Q^*): the *center* is the midpoint of the arc in the oriented face between the two green vertices.

- For faces bounded by three green vertices or more, we compute the least square plane to all vertices of the face. When a face contains an edge corresponding to a geodesic longer than π, then the middle point of this geodesic is also taken into account for computing the plane. This plane intersects the sphere in a circle. We choose the projection so that the *center* is inside the face according to the orientation given by the oriented map. The least square plane is computed using the Moore-Penrose pseudoinverse. In practice, we use the linear algebra software library Armadillo (see Sanderson and Curtin (2016)).

Note that for faces bounded by three green vertices, the *center* is the projection of the circumcenter of their triangle on the sphere, which is equidistant from all three green vertices. For more vertices, the center is thus equidistant, in a least square sense, to the vertices on the boundary of the face. Each quad face contains exactly a branch. When branches are from nearby directions, the topology remains coherent and

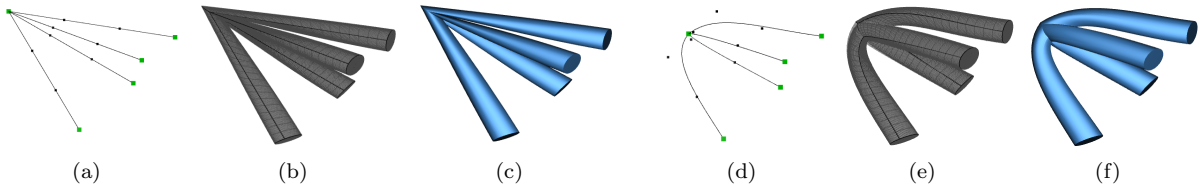

(a) (b) (c) (d) (e) (f)

Figure 6: $(a)-(c)$ A junction with four branches from nearby directions. Note that there is exactly one quad face per branch and the topology remains coherent. $(d)-(f)$ By changing the tangent of the branches, the junction is smoothed.

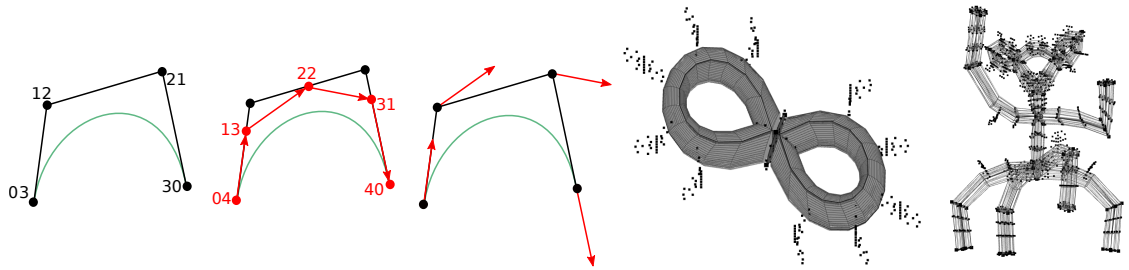

(a) (b) (c) (d) (e)

Figure 7: $(a)-(c)$: The control tangents (in red) at each Bézier control points are computed from the segment of the degree elevated control polygon (b). $(d)-(e)$: Placement of volume control points of branches.

the junction has a sharp corner. As our model offers curve branches, sharp corners can be simply avoided by smoothing the tangent direction at the junction as illustrated in Figure 6.

The order in which edges are processed at a junction affects the resulting SQS thus the kite folio that is obtained, regarding both its topology and its geometry. So, the resulting tubular object depends on this ordering. In practice, the user that is drawing a stick figure implicitly creates a total order on the edges to consider at each junction; green points are inserted in this order.

4.2.2. Geometry of branches

Each branch is attached to junctions through the kites at its extremities. We detail here the geometry criteria to ensure the best relative orientation of these two extremities. This geometric consideration completes the topological approach detailed in Section 4.1. Then, the control points of branch extremities are placed into the plane of each corresponding kite triangle. We now need to control what happens within the branch volume by defining Bézier elements between the two extremity kites. The central edge of a branch corresponds exactly to the edge in the stick figure, we then explain how we position the remaining internal control points of the branch.Two main considerations improve the geometric aspect of our branches:

- **Minimize twisting:** twisting happens when the square sections of a branch rotate around the central axis. In some extreme cases of twisting, some sections of the branch may collapse to a single point.
- **Preserve section surface:** Along a branch, the surface of the section depends on the intermediate control points. We aim here at preserving the branch section surface, that is, the thickness of the branch, in order to keep the volume distribution along the branch as constant as possible.

Coherent orienting of a branch kite

We first define the geometry criteria we use to attach the kite K of a branch to the corresponding kite $\overline{K}$ of the kite folio. In Panotopoulou et al. (2018), they propose to define a frame at each degree two vertex using Rotation Minimizing Frames (RMF); we use the same double-reflection algorithm proposed by Wang

et al. (2008) to determine the best matching between K and $\overline{K}$ according to geometry. When a branch extremity K has been identified to $\overline{K}$ and we traverse the branch for attaching the other side K' (see Section 4.1), we first compute the RMF frame from K to K'. We compute which points of K' and $\overline{K'}$ best match by choosing the points correspondence minimizing the total distance between corresponding points. We consider identifying points of similar colors (that is, we choose one of the two possible configurations). When the branch is the first to be attached on the kite folio hosting K', we also consider a red/blue swapping of the SQS (that leads to choosing the best configuration among four possible). This minimizes the twist at K', thus along the branch. After this step, the parametric domain defined by the semi-simploidal set is entirely defined, and thus the set of control points to be embedded in 3D.

Defining control points along a branch

The control points of branch extremities are now positioned according to the kites, and the control points of the central Bézier curve c of the branch are mapped to the control point of the stick figure. In order to define the branch section around c, we need a frame along c to determine the set of control points to be embedded in 3D. We now determine the internal control points of the Bézier volume elements, aiming to ensure consistent volume distribution along the branch. A first idea is to place the internal control points of a branch by interpolating the control points between the starting and ending kites control points. This idea would be adapted for straight branches. For a non linear curve c, in order to prevent a flattening of the branch, the slices of control points need to be as orthogonal to the curve as possible – when a slice of control points becomes tangent to the curve, the corresponding part of the branch flattens. We thus define a local frame at each internal control point of c. Note that the rotation minimizing frames are a priori defined on the curve and not for the control points. Nevertheless the double-reflection algorithm Wang et al. (2008) only needs the tangent at a point to compute its local frame. In order to define a rotation minimizing frame for each internal control point we thus need a tangent at each control point. A Bézier control polygon with $n+1$ control points converges smoothly to its curve Morin and Goldman (2001), but has n control tangents. We use degree elevation to associate a tangent to each control point: we can deduce $n+1$ control tangents, thus, a frame per internal control points (see Figure 7 $(a)-(c)$). Interpolating the intermediate control points and expressing them into this local frame gives our branches a more intuitive (and not flattened) shape (see Figure 7 (d)).

This last step completes the automatic process for creating the volume model from the stick figure.

4.3. Results

Figure 8 shows piecewise polynomial volumes we automatically generate from the stick figures on the left. We focus in particular in challenging situations regarding topology. The first example contains cycles, and all vertices of the stick graph are of degree at most 3. The second and third examples: a clover and an octopus has a central vertex of degree 9, and contains double edges. The last example, the snake, contains loops and curves of different degrees, and illustrates the smoothness of the proposed polynomial model.

5. Conclusion and Future Work

In this paper, we proposed a method for generating tubular piecewise polynomial volume objects from stick figures. We show that semi-simploidal sets can directly be used for handling both topology and geometry of volume tubular objects, providing a consistent structure together with a parametric domain for Bézier embedding.

We propose a branch structure made of four prisms which preserves the minimal number of cells on the object surface. If hexahedral volumes are needed, the presented approach still holds using a branch structure made of four hexahera (as cubes are also simploids). However, in this case, the boundary surface would have twice the number of quads.

The structure of junctions are defined by their corresponding SQS. In our approach, SQS are obtained by considering green points sequentially, so given a set of green points, different SQS may be obtained depending on the chosen order. It would be interesting to find a canonical SQS for a given set of green points, i.e.,

independent of ordering. In this case, a global optimization approach could be considered for defining the topology and the geometry of the sphere quadrangulation. We do not consider here the possible collisions between different parts of the model. It would be interesting to link geometric properties of the skeleton to prevent intersection of the model, and place the Bézier volume control points to avoid the geometric singularities despite the smoothness of the parameterized volume. We would also like to investigate varying thickness within the model. Branches could have different and varying thickness. This would implies an adaptation of junction handling.

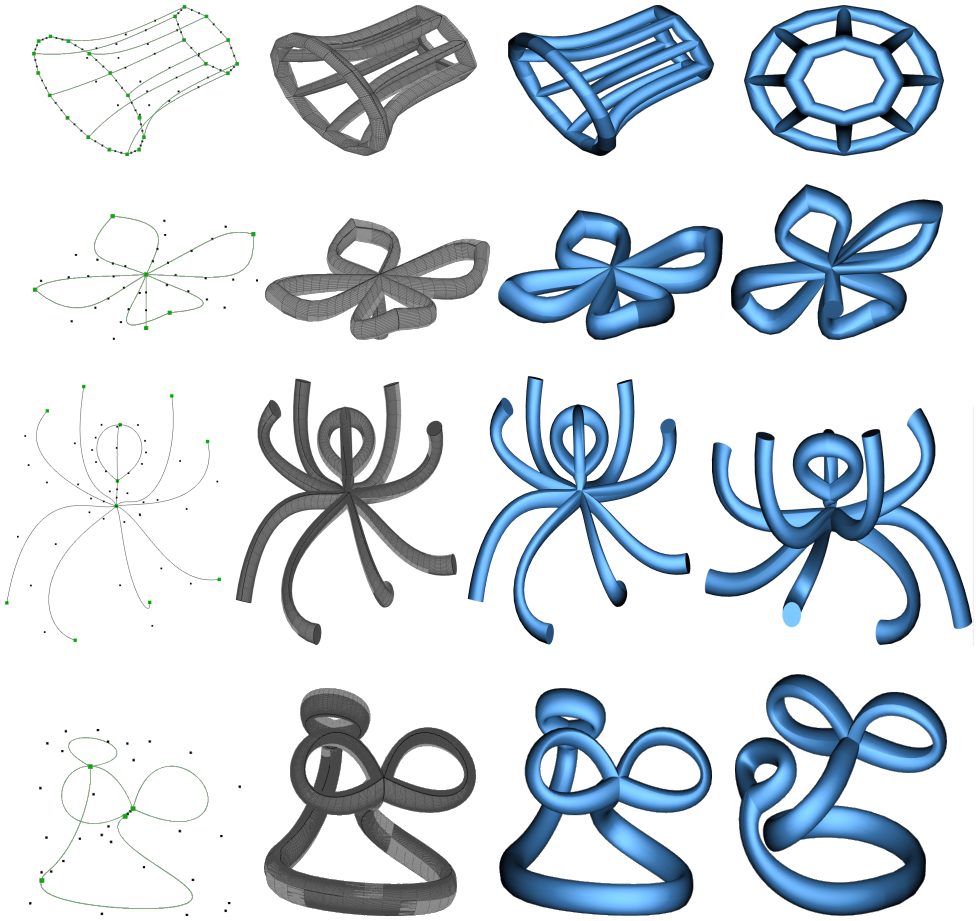

Figure 8: From left to right: stick figures made of Bézier curves in green; the control points are the black dots, then 3D volume meshes, volume object rendered, and another view of the same object. Even if performance is not a main keypoint of this work, we provide the computation time for this volume models: 750ms for the bin (first row), 117ms for the clover (second row), 80ms for the snake (third row) and 175ms for the octopus (last row).

Acknowledgements

The authors gratefully acknowledge Pascal Lienhardt for helpful discussions. This work benefited from government support managed by the National Research Agency under the *Investments for the future* program with the reference ANR-10-LABX-0074-01 Sigma-LIM.

References

Batagelj, V., 1989. An inductive definition of the class of 3-connected quadrangulations of the plane. Discrete Mathematics 78, 45–53. Special Double Issue in Memory of Tory Parsons.

Brinkmann, G., Greenberg, S., Greenhill, C., McKay, B.D., Thomas, R., Wollan, P., 2005. Generation of simple quadrangulations of the sphere. Discrete Mathematics 305, 33–54. doi:https://doi.org/10.1016/j.disc.2005.10.005.

Brown, R., Higgins, P.J., 1981. On the algebra of cubes. Journal of Pure and Applied Algebra 21, 233 – 260.

Bærentzen, J., Misztal, M., Wełnicka, K., 2012. Converting skeletal structures to quad dominant meshes. Computers & Graphics 36, 555 – 561. doi:https://doi.org/10.1016/j.cag.2012.03.016. shape Modeling International (SMI) Conference 2012.

Cottrell, J.A., Hughes, T.J., Bazilevs, Y., 2009. Isogeometric analysis: toward integration of CAD and FEA. John Wiley & Sons.

Dahmen, W., Micchelli, C.A., 1982. On the linear independence of multivariate b-splines I. Triangulation of simploids. SIAM J. Numer. Anal. 19.

Damiand, G., Lienhardt, P., 2014. Combinatorial Maps: Efficient Data Structures for Computer Graphics and Image Processing. A K Peters/CRC Press.

DeRose, T., Goldman, R.N., Hagen, H., Mann, S., 1993. Functional composition algorithms via blossoming. Transactions On Graphics 12, 113–135.

Dobkin, D., Laszlo, M., 1987. Primitives for the manipulation of three-dimensional subdivisions, in: 3rd Symposium on Computational Geometry, Waterloo, Canada. pp. 86–99.

Edmonds, J., 1960. A combinatorial representation for polyhedral surfaces. Notices Amer. Math. Soc. 7, 646.

Eilenberg, S., Zilber, J., 1950. Semi-simplicial complexes and singular homology. Annals of Mathematics 51, 499–513.

Farin, G., 2014. Curves and surfaces for computer-aided geometric design: a practical guide. Elsevier.

Fuentes Suárez, A., Hubert, E., 2018. Scaffolding skeletons using spherical voronoi diagrams: Feasibility, regularity and symmetry. Computer-Aided Design 102, 83 – 93. doi:https://doi.org/10.1016/j.cad.2018.04.016. proceeding of SPM 2018 Symposium.

Guibas, L., Stolfi, G., 1985. Primitives for the manipulation of general subdivisions and the computation of voronoi diagrams. Transactions on Graphics 4, 74–123.

Hatcher, A., 2002. Algebraic Topology. Cambridge University Press.

Hughes, T., Cottrell, J., Bazilevs, Y., 2005. Isogeometric analysis: Cad, finite elements, nurbs, exact geometry and mesh refinement. Computer Methods in Applied Mechanics and Engineering 194, 4135–4195. doi:https://doi.org/10.1016/j.cma.2004.10.008.

Lang, V., Lienhardt, P., 1996. Simplicial sets and triangular patches, in: Computer Graphics International Conference, CGI 1996, Pohang, Korea, June 24-28, 1996, pp. 154–163.

Lienhardt, P., 1989. Subdivisions of n-dimensional spaces and n-dimensional generalized maps, in: ACM Symposium on Computational Geometry, pp. 228–236.

Lienhardt, P., 1991. Topological models for boundary representation: a comparison with n-dimensional generalized maps. Computer-Aided Design 23, 59–82. doi:https://doi.org/10.1016/0010-4485(91)90082-8.

Livesu, M., Ellero, S., Martínez, J., Lefebvre, S., Attene, M., 2017. From 3d models to 3d prints: an overview of the processing pipeline, in: Computer Graphics Forum, Wiley Online Library. pp. 537–564.

Livesu, M., Muntoni, A., Puppo, E., Scateni, R., 2016. Skeleton-driven adaptive hexahedral meshing of tubular shapes. Computer Graphics Forum 35, 237–246. doi:10.1111/cgf.13021.

Lyon, M., Bommes, D., Kobbelt, L., 2016. Hexex: robust hexahedral mesh extraction. ACM Transactions on Graphics (TOG) 35, 1–11.

Mäntylä, M., 1988. An Introduction to Solid Modeling. Computer Science Press,.

Massarwi, F., Antolin, P., Elber, G., 2019. Volumetric untrimming: Precise decomposition of trimmed trivariates into tensor products. Computer Aided Geometric Design 71, 1–15.

Massarwi, F., Elber, G., 2016. A b-spline based framework for volumetric object modeling. Computer-Aided Design 78, 36–47.

Morin, G., Goldman, R., 2001. On the smooth convergence of subdivision and degree elevation for bézier curves. Computer Aided Geometric Design 18, 657–666.

Munkres, J.R., 1984. Elements of algebraic topology. Perseus Books.

Nakamoto, A., 1996. Diagonal transformations in quadrangulations of surfaces. Journal of Graph Theory 21, 289–299. doi:https://doi.org/10.1002/(SICI)1097-0118(199603)21:3<289::AID-JGT3>3.0.CO;2-M.

Panotopoulou, A., Ross, E., Welker, K., Hubert, E., Morin, G., 2018. Scaffolding a skeleton, in: Research in Shape Analysis. Springer, pp. 17–35.

Peltier, S., Fuchs, L., Lienhardt, P., 2009. Simploidals sets: Definitions, operations and comparison with simplicial sets. Discrete App. Math. 157, 542–557 (extended version of "Homology of Simploidal Sets", DGCI 2006, Szeged, Hungary, 235–246).

Peltier, S., Lienhardt, P., 2018. Simploidal Sets: a data structure for handling simploidal Bezier spaces. Computer Aided Geometric Design 62, 44 – 62. doi:10.1016/j.cagd.2018.03.010.

Raptis, M., Kirovski, D., Hoppe, H., 2011. Real-time classification of dance gestures from skeleton animation, in: Proceedings of the 2011 ACM SIGGRAPH/Eurographics symposium on computer animation, pp. 147–156.

Sanderson, C., Curtin, R., 2016. Armadillo: a template-based c++ library for linear algebra. Journal of Open Source Software 1, 26.

Sundar, H., Silver, D., Gagvani, N., Dickinson, S., 2003. Skeleton based shape matching and retrieval, in: 2003 Shape Modeling International., IEEE. pp. 130–139.

Usai, F., Livesu, M., Puppo, E., Tarini, M., Scateni, R., 2016. Extraction of the quad layout of a triangle mesh guided by its curve skeleton. ACM Trans. Graph. 35. doi:10.1145/2809785.

Vince, A., 1983. Combinatorial maps. Journal of Combinatorial Theory 34, 1–21.

Wang, W., Jüttler, B., Zheng, D., Liu, Y., 2008. Computation of rotation minimizing frames. ACM Transactions on Graphics (TOG) 27, 1–18.

Weiler, K., 1985. Edge-based data structures for solid modelling in curved-surface environments. Comput. Graph. Appl. 5, 21–40.